THE ASTROPHYSICAL JOURNAL, 433:117–130, 1994 September 20

DENSE CORES IN DARK CLOUDS. X. AMMONIA EMISSION IN THE PERSEUS MOLECULAR CLOUD COMPLEX

E. F. LADD
Institute for Astronomy, University of Hawaii, 2680 Woodlawn Drive, Honolulu, HI 96822;
ladd@galileo.ifa.hawaii.edu

AND

P. C. MYERS AND A. A. GOODMAN
Harvard-Smithsonian Center for Astrophysics, Mail Stop 42, 60 Garden Street, Cambridge, MA 02138
Received 1993 October 25; accepted 1994 March 1

ABSTRACT

We present a survey for dense material around young *IRAS* sources in the Perseus molecular cloud complex in the NH_3 $(J, K) = (1, 1)$ line at 1.3 cm. NH_3 emission was detected in eight, and mapped in seven, out of 10 positions chosen for study. The dense cores found typically have lower masses and narrower line widths than cores previously studied in Perseus and are located near sources of lower luminosity. NH_3 cores are found throughout the Perseus complex; however, much of the detected dense gas is concentrated into two filamentary "ridges" located in the western part. As a group, NH_3 cores in Perseus have a mean line width of 0.6 km s^{-1}, mean radius of 0.12 pc, mean kinetic temperature of 13 K, and mean mass of 9 $M_\odot$. These mean values are larger than the mean values for NH_3 cores with associated stars in Taurus, but smaller than the mean values for cores associated with stars in Orion A. Some of the cores in Perseus are "thermally dominated," with thermal and nonthermal line widths similar to most Taurus cores, while others are "nonthermally dominated" and are more similar to the cores in Orion A. We conclude that the Perseus complex is intermediate in its star-forming potential between the predominantly low-mass star-producing regions like Taurus and the regions capable of the producing high-mass stars such as Orion A.

Subject headings: ISM: individual (Perseus molecular cloud) — ISM: molecules — radio lines: ISM

1. INTRODUCTION

Stars form in dense condensations within molecular clouds. These condensations have large column densities ($N_{H_2} \gtrsim 10^{22}$ cm^{-2}) and gas densities ($n_{H_2} \gtrsim 10^4$ cm^{-3}), making them opaque both visually and in the lines of CO, a common tracer of molecular cloud material. To study the contents and properties of these dense cores, then, one must observe at other wavelengths, where these cores are less opaque.

The spectral lines of the 23 GHz inversion transition of NH_3 have proved to be good tracers of the densest material in dense cores, particularly those forming low-mass stars (see, e.g., Ho & Townes 1983; Benson & Myers 1989). The upper levels of the rotational ladder are collisionally populated significantly only within regions of relatively high volume density ($n_{H_2} \gtrsim 3 \times 10^3$ cm^{-3}), so emission is observed only toward high-density material. The $(J, K) = (1, 1)$ transition has 18 hyperfine components, grouped into five spectrally distinct groups, allowing for determination of the optical depth of the emission. Furthermore, the $(J, K) = (2, 2)$ lines are shifted in frequency from the (1, 1) lines by less than 1 GHz, and therefore both transitions can be observed with the same telescopes and receiver configurations, allowing for more accurate determinations of excitation and kinetic temperatures.

NH_3 emission has been observed toward a variety of dense cores, from small "starless" cores that may or may not ever produce a star, to cores containing individual young stars, and cores containing young star clusters with O and B stars (Ho & Townes 1983; Myers, Ladd, & Fuller 1991). Observations indicate that the mass, line width, and temperature of an NH_3 core increases with the luminosity of the embedded source or sources (Wouterloot, Walmsley, & Henkel 1988; Stacy et al. 1988; Ladd 1991; Myers et al. 1991). Myers et al. (1991) showed that NH_3 cores can be described as thermally or nonthermally dominated, depending on whether the thermal line width, inferred from the kinetic temperature, exceeds the nonthermal line width, determined from the observed line width. They showed that cores containing embedded sources with luminosity less than ~ 10 $L_\odot$ are generally thermally dominated, while cores with luminosity greater than ~ 10 $L_\odot$ are generally nonthermally dominated.

The Perseus molecular cloud complex is interesting because there exist young sources with luminosities both greater and less than 10 $L_\odot$. The infrared survey of Ladd, Lada, & Myers (1993) showed that Perseus contains embedded sources ranging in luminosity from 0.6 to 320 $L_\odot$ and suggested that Perseus is intermediate in its star-forming properties between the Taurus complex, where stars predominantly appear to form in relative isolation (YSO surface density ~ 10 pc^{-2}), and the Orion complex, where the dominant mode of star formation involves large clusters with densities of 100 pc^{-2}. In this work, we examine the properties of the dense gas in the Perseus complex and compare the Perseus cores in Taurus and Orion.

The Perseus molecular cloud complex is a conglomeration of regions of high visual extinction extending over some 9° at a Galactic longitude of ~ 160 degrees and latitude ranging from $-23°$ to $-14°$. Its high Galactic latitude and its low LSR velocity determined from observations of CO (Sargent 1976) and ^{13}CO (Bachiller & Cernicharo 1986) suggest that it is within a few hundred parsecs of the Sun, though its actual distance is somewhat controversial. Most authors agree that it is associated with the Per OB2 association, whose distance has been estimated to be 334 ± 12 pc (Borgman & Blaauw 1964).

However, Lynds (1969) notes that the dark-cloud complex is probably in front of the OB association and that 350 pc is probably an upper limit to the dark-cloud distance.

The complex has been observed in lines of CO (Sargent 1976; Ungerechts & Thaddeus 1986) and ^{13}CO (Bachiller & Cernicharo 1986; Bally 1991), and its visual extinction has been estimated using star counts (Cernicharo & Bachiller 1984). It is extended over 15 × 55 pc (Sargent 1976), and the total mass of gas in the region is estimated as $2 \times 10^4\ M_\odot$, assuming a distance of 350 pc (Cernicharo, Bachiller, & Duvert 1985). An east-west gradient in LSR velocity is seen in several lines with velocity increasing to the east. Sargent (1976) concludes that the velocity gradient does not result from a single object, but rather a series of distinct clumps at slightly different velocities. Cernicharo et al. (1985) suggest that there are two distinct clouds, one located at a distance comparable to that of the Taurus complex (~200 pc), and a second layer at ~300 pc, the distance of the Per OB2 association. However, the higher spatial resolution ^{13}CO mapping of Bally (1991) appears to show that, while the velocity structure is complex and filamentary, there is a smooth progression in velocity from east to west for the bulk of the gas.

Most measurements of stars believed to be associated with the complex yield distances of 350–500 pc, similar to that derived by Borgman & Blauuw (1964) for the Per OB2 association (see, e.g., Harris, Morgan, & Roman 1954; Strom, Grasdalen, & Strom 1974; Herbig & Jones 1983). Based on these results, we adopt a distance of 350 pc.

The complex contains six well-studied regions of star formation activity—L1448 (see, e.g., Bachiller et al. 1990a; Anglada et al. 1989; Levreault 1985), L1455 (e.g., Heyer et al. 1986; Schwartz, Frerking, & Smith 1985; Davidson & Jaffe 1984; Goldsmith et al. 1984), NGC 1333 (e.g., Loren, Vanden Bout, & Davis 1973; Loren 1976; Ho & Barrett 1980; Schwartz, Waak, & Smith 1983; Strom, Vrba, & Strom 1976; Harvey, Wilking, & Joy 1984), B1 (e.g., Bachiller, Menten, & del Rio-Alvarez 1990b; Bachiller, Martin-Pintado, & Planesas 1991; Cohen & Kuhi 1979; Goodman et al. 1989), IC 348 (e.g., Blaauw 1952; Bachiller, Guilloteau, & Kahane 1987; Strom, Strom, & Carrasco 1974), and B5 (e.g., Goldsmith, Langer, & Wilson 1986; Langer et al. 1989; Benson & Myers 1989; Fuller et al. 1991)—and a small collection of individual emission line stars (Herbig & Bell 1988). Two of these star formation regions, NGC 1333 and IC 348, are particularly bright and contain newly formed intermediate-mass stars of spectral type B, as well as a cluster of young stars of lower masses. The brightest sources in the other four regions have significantly lower luminosity than do B stars.

Parts of the Perseus complex have been searched previously for NH_3, but no systematic, cloudwide study has been reported. In this paper we present the results of an *IRAS*-based search for NH_3 emission throughout the complex. In § 2 we describe the observational method, search list, and initial data reduction. In § 3 we compare our results with previous NH_3 work in Perseus and produce a Perseus core sample for comparison with Taurus and Orion. In § 4 we discuss the comparison between Perseus, Taurus, and Orion, in terms of both the dense gas content and young stellar populations. We present our conclusions in § 5.

2. OBSERVATIONS

We observed the sources in the Perseus complex in the $(J, K) = (1, 1)$ 23.7 GHz inversion transition of NH_3 at the 37 m telescope of the Haystack Observatory[1] in Westford, MA, during seven multiday observing sessions in 1988 December, 1989 June, 1990 February, 1990 July, 1991 February, 1992 June, and 1992 December. Our observations were frequency switched by 0.11 MHz to remove atmospheric and instrumental contributions. The measured full width at half-maximum (FWHM) beam size was 88″. We used three detection configurations during the survey. Some of the observations were made with a single-maser receiver and with either a 6.66 MHz or 4.44 MHz bandwidth and 1024 channel autocorrelator, which resulted in FWHM velocity resolution of 0.12 km s^{-1} and 0.08 km s^{-1}, respectively. Other observations used a two-maser system, which detected orthogonal linear polarizations through two 3.2 MHz bands and split the autocorrelator into two 512 channel systems. These observations have FWHM velocity resolution of 0.12 km s^{-1}. System temperatures ranged from 55 to 100 K during the winter observations and from 85 to 150 K in the summertime. In all cases, spectra were integrated until the rms antenna temperature (T_A^*) was less than 0.1 K (typically 30 minutes in winter and 60 minutes in summer), and in most cases, less than 0.05 K.

The spectral intensities were corrected for variation in atmospheric attenuation and antenna gain with elevation. The antenna surface was modified on several occasions over the course of these observations, and the gain dependence on elevation was remeasured after each rerigging of the antenna. We determined the gain correction by observing a source of known brightness (B5; Benson & Myers 1989), and by regular monitoring of one of our stronger detections (Per 6 [0–1]; the numbers in brackets indicate the offset in arcminutes from the map center position) at a variety of elevations and during varied weather conditions. We assume a telescope beam efficiency of 0.25. From these measurements, we estimate that the corrected line antenna temperatures T_A^* are reproducible at the 20% level.

Pointing corrections as a function of both azimuth and elevation from the standard Haystack pointing map were used for all the observations. We monitored the telescope pointing by observing continuum point sources (usually 3C84) frequently during our observing sessions. We consistently found pointing errors $<35''$, and typically $<20''$ (<0.2 times the FWHM beam width).

In the six brightest cores we detected, we observed nine positions with strong (1, 1) lines in the $(J, K) = (2, 2)$ 23.7 GHz inversion transition. We used the single-maser system described above with the 4.44 MHz bandwidth and hence a FWHM velocity resolution of 0.08 km s^{-1}. These observations were conducted under excellent weather conditions in 1991 February, and all the (2, 2) spectra have rms noise levels <0.04 K.

Our source list was constructed from a comparison between the *IRAS* Point Source Catalog, Version 2 (1988; hereafter PSC) and the visual extinction maps of Cernicharo & Bachiller (1984). We selected all PSC sources with $S_{100\mu m} > S_{60\mu m}$, located within 0.4 pc (in projection) of an extinction peak whose maximum extinction exceeds $A_V = 4$. We did not discriminate on the basis of PSC data quality. The resulting source list contains 13 PSC objects. Three sources, IRAS 03245+3002 (L1455; Anglada et al. 1989), IRAS 03301+3057 (B1; Bachiller et al. 1990a), and IRAS 03271+3013; (Bachiller

[1] Radio astronomy at the Haystack Observatory of the Northeast Radio Observatory Corporation is supported by the National Science Foundation.

TABLE 1

IRAS PSC SOURCES SEARCHED FOR NH_3

PSC NAME	R.A. (1950)	Decl. (1950)	CORE NAME	No. OF POSITIONS	POSITION OF PEAK T_A^* ([α, δ])	GAUSSIAN FITS[a] T_A^* (K)	V_{LSR} (km s^{-1})	ΔV (km s^{-1})	rms (K)
03213+3102.....	20.2	17″	Per 1	14	[1, 0]	0.16	4.09	0.84	0.028
03256+3016.....	40.6	31	[d]	5	...	...	...	...	0.021
03256+3055.....	39.2	20	Per 3	28	[0, 0]	0.76	7.27	0.80	0.042
03262+3123.....	16.8	13	Per 4	49	[−1, −6]	0.60	7.50	0.68	0.063
03267+3128.....	45.5	48	Per 5	16	[0, 0]	0.76	8.13	0.67	0.031
03271+3013.....	10.3	34	Per 6[c]	21	[0, −1]	0.82	5.80	0.70	0.048
03295+3050.....	30.3	50	Per 7	27	[2, −1]	0.60	6.71	0.82	0.024
03303+3108.....	19.6	14	Per 9	27	[−2, 2]	0.61	6.92	0.54	0.10
03380+3135.....	1.6	2	Per 10	5	[0, 1]	0.1	7.81	1.5	0.030
03406+3144.....	39.8	2	[d]	4	...	...	...	...	0.040

[a] Results listed are for a single Gaussian fit to the blended main group of hyperfine components.
[b] Entries indicate the offset from the *IRAS* position to the positions of peak T_A^* in arcminutes of right ascension and declination.
[c] Observed in NH_3 previously by Bachiller et al. 1991.
[d] No NH_3 was detected toward this source.

et al. 1991; Tafalla et al. 1993) have been observed in NH_3 previously. We also mapped the region around IRAS 03271+3013 but did not remap the regions around the other two sources. We observed the remaining objects, except IRAS 03255+3103 (however, see Knee, Cameron, & Liseau 1990 for a CS map) in the survey presented here. Table 1 contains our source list.

3. OBSERVED CORE PROPERTIES

Out of 10 positions surveyed, eight had detectable NH_3 emission with $T_A^* \geq 0.1$ K. The number of positions surveyed toward each *IRAS* PSC source and the position of the peak T_A^* are listed in Table 1, along with the T_A^*, line center velocity (V_{LSR}), and line width (ΔV) derived from a single Gaussian fit to the blended main group of hyperfine components. The positions of these detections and the upper limits are overlaid on the ^{13}CO map of Bachiller & Cernicharo (1986) in Figure 1, along with the positions of previously studied NH_3 cores in Perseus.

3.1. *Spectral Properties*

The NH_3 emission from nine positions in six cores was bright enough to permit a detailed modeling of the hyperfine structure as described by Benson & Myers (1989). The least-squares fit of the model spectrum to the observed spectrum determines the center velocity, the intrinsic line width, the total (1, 1) optical depth, and the (1, 1) excitation temperature. The beam filling factor, Φ, was estimated from our maps. The results of this fitting are displayed in Table 2. Nine positions were also observed in the $(J, K) = (2, 2)$ transition. From the

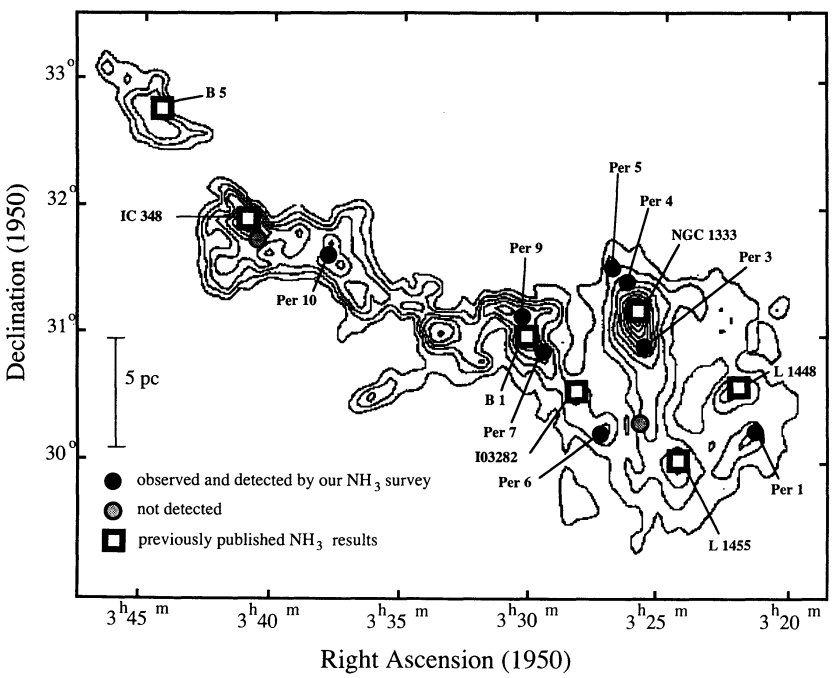

FIG. 1.—Search positions for our NH_3 survey overlaid on the ^{13}CO map of Bachiller & Cernicharo (1986). Black circles indicate detections; shaded circles indicate nondetections. Previously mapped NH_3 cores are indicated by white boxes.

TABLE 2

PARAMETERS DERIVED FROM DETAILED FITS TO SPECTRA

Name	V_{LSR} (km s^{-1})	ΔV (km s^{-1})	Φ	τ	T_{ex} (K)	T_K (K)	log n (cm^{-3})	log N_{NH_3} (cm^{-2})
Per 3 [0, 0]	7.03(1)	0.39(2)	0.8	6.0(7)	6.1(1)	11(2)	4.18(3)	14.1(7)
Per 3 [−2, −1]	6.83(1)	0.62(1)	0.8	3.9(2)	6.4(1)	11(3)	4.24(4)	14.1(9)
Per 4 [0, 0]	7.53(1)	0.31(1)	0.9	5.1(6)	5.1(2)	10(3)	4.00(6)	14(1)
Per 4 [−1, −4]	7.58(1)	0.27(1)	1.0	3.9(7)	5.0(6)	9(3)	4.0(1)	14(1)
Per 5 [0, 0]	8.25(1)	0.31(1)	0.5	4.3(6)	9.8(2)	11(6)	5.03(5)	14(2)
Per 6 [0, 0]	8.09(1)	0.31(1)	0.7	6.8(6)	6.5(3)	11(3)	4.27(5)	14(1)
Per 7 [2, −1]	6.80(1)	0.42(2)	0.7	5.8(5)	5.8(1)	11(2)	4.12(4)	14.1(6)
Per 7 [−2, −1]	6.47(1)	0.37(2)	1.0	6(1)	4.3(2)	11(4)	3.70(7)	14(1)
Per 9 [−3, 2]	6.90(1)	0.40(2)	0.7	7.1(7)	5.5(1)	11(1)	4.06(2)	14.2(5)

NOTE.—Numbers in parentheses are the errors in the least significant digit listed. Errors in V_{LSR}, ΔV, τ, and T_{ex} are the 1 σ errors from the 18-component fit. Errors in T_K, log n, and log N_{NH_3}, result from formal propagation of the errors in V_{LSR}, ΔV, τ, and T_{ex} (see text).

(1, 1) and (2, 2) spectra at these positions, we have calculated the kinetic temperature (T_k), total volume density (n), and NH_3 column density (N_{NH_3}) using the method of Benson (1983). The best-fit values for these parameters, along with their 1 σ errors are listed in Table 2.

3.2. *Map Properties*

We have mapped the (1, 1) emission in seven of the eight new cores. Maps were extended at least to half-power, typically with 10 measurements within the half-maximum contour. For the eighth core, Per 10, NH_3 emission was sought in five positions but detected at only one. The main (1, 1) component of each spectrum was fit with a single Gaussian to determine the antenna temperature (T_A^*), LSR velocity, and observational line width at each position. The T_A^* maps are shown in Figures 2–8. The *IRAS* position is noted in each map as the [0, 0] position.

The maps can be divided into two groups, based on their morphology: (1) maps that have a single maximum (Per 1, Per 3, Per 5, and Per 6), and (2) those that have multiple peaks connected by low-level emission (Per 4, Per 7, and Per 9). Each source in the first group is centered or nearly centered on its associated *IRAS* source position. Several of them are barely resolved in one direction. Per 1 and Per 5 in particular are almost point sources. The sources in the second group are not centered on their respective *IRAS* positions, with the exception of Per 4, where one of the peaks is centered on the *IRAS* position. The individual peaks in these sources are also very small, but there is considerable low-level emission extending for several beams.

Because many of these maps are multipeaked, we estimate their size r as

$$r = \left[\left(\frac{A}{\pi}\right) - \left(\frac{D\Theta}{2}\right)^2\right]^{0.5}, \quad (1)$$

where A is the area within the half-maximum contour, Θ is the FWHM beam size of the observations (88″), and D is the

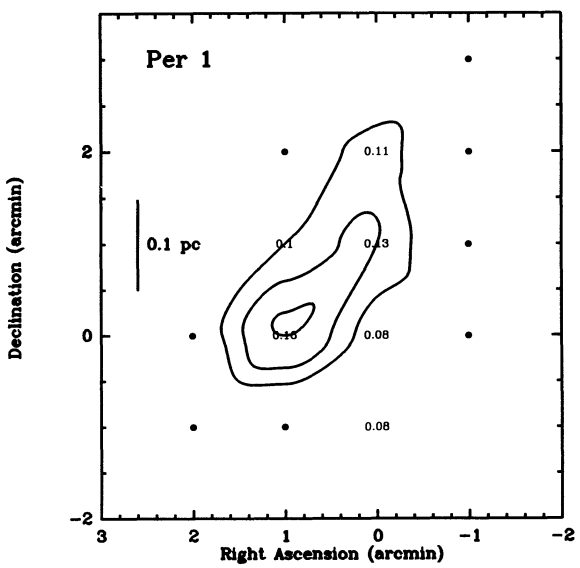

FIG. 2.—Contour map of T_A^* toward Per 1. Detections are labeled with their values, and nondetections are listed as filled dots. Contour levels are 0.1, 0.13, and 0.16 K. The [0, 0] position is ($3^h21^m20^s.2$, 31°2′17″).

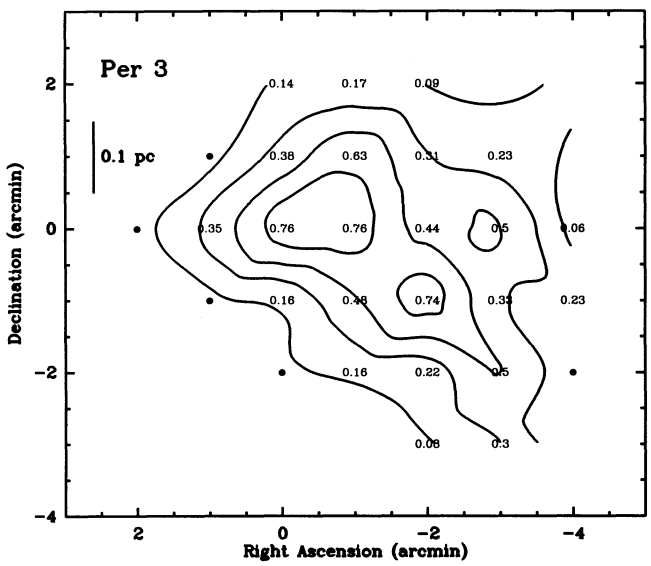

FIG. 3.—Contour map of T_A^* toward Per 3. Detections are labeled with their values, and nondetections are listed as filled dots. Contour levels are 0.1, 0.3, 0.5, and 0.7 K. The [0, 0] position is ($3^h25^m39^s.2$, 30°55′20″).

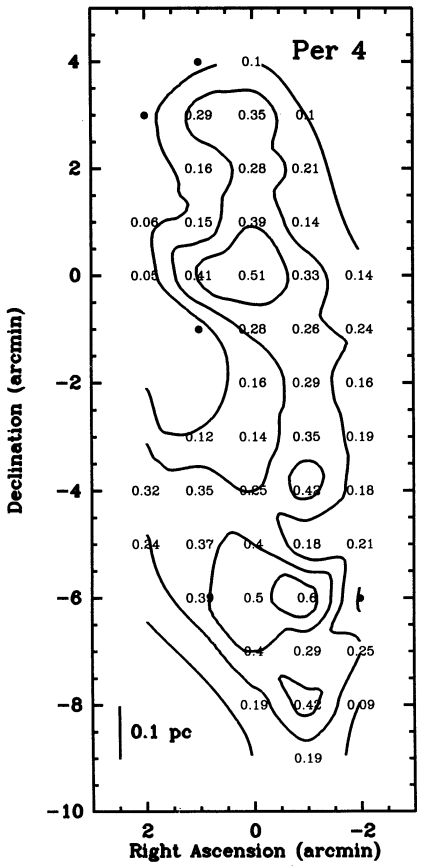

FIG. 4.—Contour map of T_A^* toward Per 4. Detections are labeled with their values, and nondetections are listed as filled dots. Contour levels are 0.1, 0.25, 0.4, 0.55, and 0.7 K. The [0, 0] position is ($3^h26^m16^s.8$, 31°23′13″).

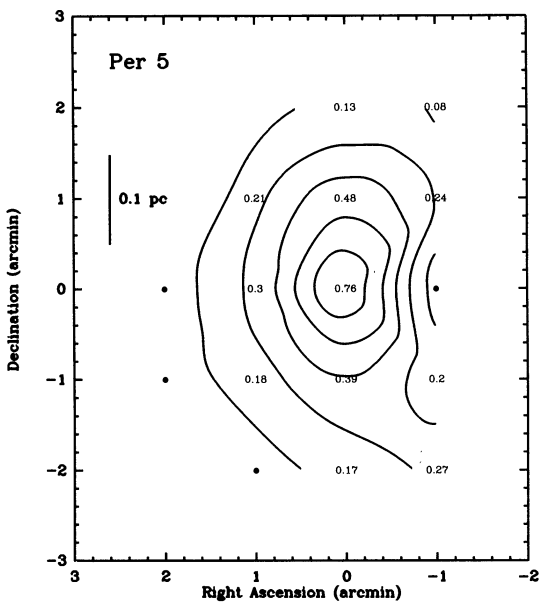

FIG. 5.—Contour map of T_A^* toward Per 5. Detections are labeled with their values, and nondetections are listed as filled dots. Contour levels are 0.1, 0.25, 0.4, 0.55, and 0.7 K. The [0, 0] position is ($3^h26^m45^s.5$, 31°28′48″).

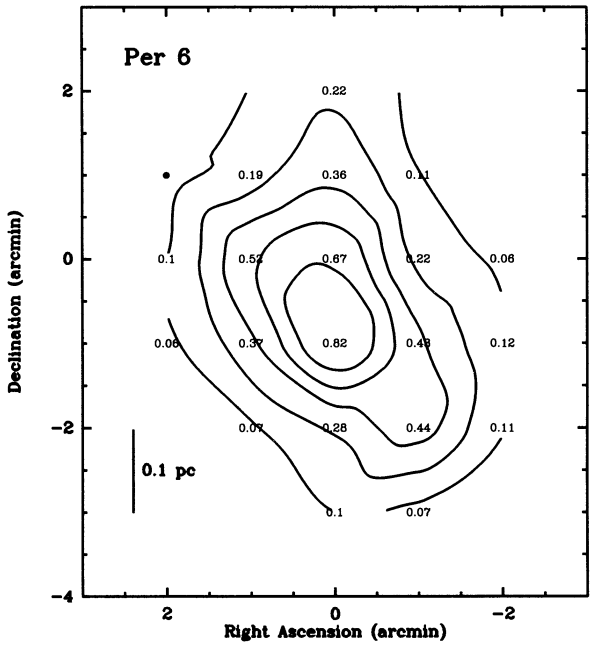

FIG. 6.—Contour map of T_A^* toward Per 6. Detections are labeled with their values, and nondetections are listed as filled dots. Contour levels are 0.1, 0.25, 0.4, 0.55, 0.7, and 0.85 K. The [0, 0] position is ($3^h27^m10^s.3$, 30°13′34″).

assumed distance to the Perseus complex (350 pc).[2] Since the peaks in the multiply-peaked maps are typically not separated at half-power, we calculate r in the following two ways. First, we estimate r from the entire map, using the value of the brightest detection to determine the half-power contour. Then we estimate r for each clump based on its half-power contour. Where the half-power contours are not closed around a single

[2] This method for determining core size has been used by Cesaroni & Wilson (1994), but differs slightly from the method used by Benson & Myers (1989) and Harju, Walmsley, & Wouterloot (1991), who fit the maps with elliptical Gaussians and quote the geometric mean of the deconvolved major and minor axes. The differences between the sizes derived by these two methods exceeds 10% only if the cores are not well resolved (i.e., map minor axis $\lesssim 1.5\Theta$) *and* the aspect ratio of the map is greater than 5.

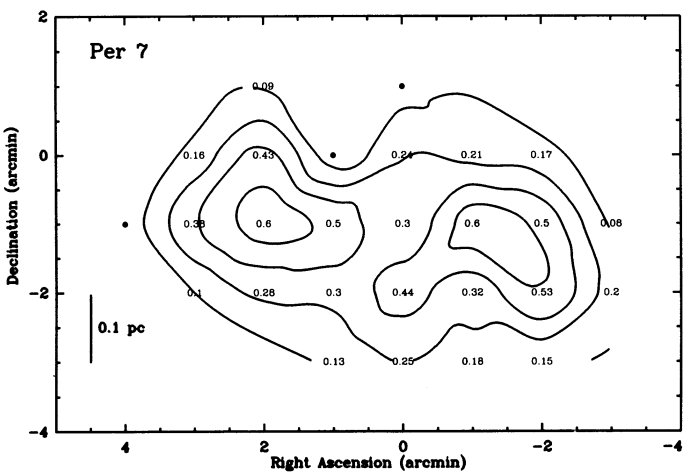

FIG. 7.—Contour map of T_A^* toward Per 7. Detections are labeled with their values, and nondetections are listed as filled dots. Contour levels are 0.1, 0.25, 0.4, and 0.55 K. The [0, 0] position is ($3^h29^m30^s.3$, 30°50′50″).

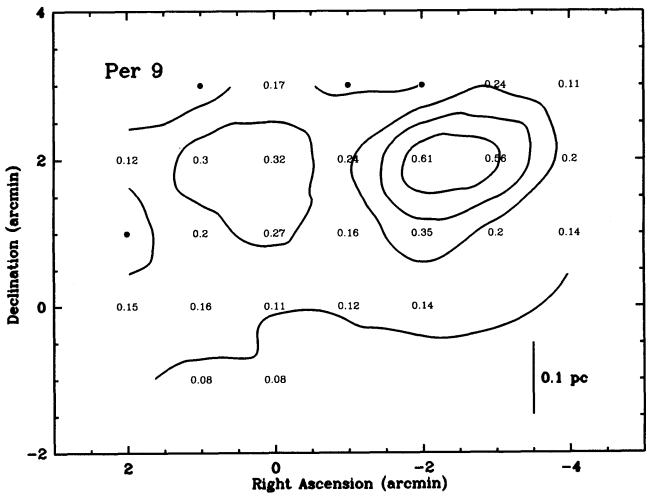

FIG. 8.—Contour map of T_A^* toward Per 9. Detections are labeled with their values, and nondetections are listed as filled dots. Contour levels are 0.1, 0.25, 0.4, and 0.55 K. The [0, 0] position is ($3^h30^m19^s.6$, 31°8′14″).

clump, we have divided the map at the saddle point between clumps. Values for r using both methods are listed in Table 3. Errors are estimated by propagating the map rms error into our estimate for r.

We then calculate two values for the mass of each clump—a mass M_N based on the measured column density and r, and a mass M_n based on the volume density and r:

$$M_n = 2.3 \frac{4\pi}{3} n m_p r^3 \quad (2)$$

and

$$M_N = 2.3 \frac{2\pi}{3} N m_p r^2 , \quad (3)$$

where m_p is the mass of a proton and the factor of 2.3 accounts for the presence of helium and other metals. We have assumed that N is the maximum column density in a constant-density sphere of density n and radius r and that the abundance of NH_3 relative to H_2 is 10^{-7}. This abundance is similar to that found by Bachiller et al. (1987), (1991) for other cores in Perseus and is consistent with our estimates for the volume density and size of the cores presented here (i.e., $nr \simeq 10^{-7} N_{NH_3}$.)

This formulation is slightly different from that used by Benson & Myers (1989) in that we use the radius rather than the diameter of the circulated FWHM contour as the radius of the sphere used to calculate the total mass. Hence M_n calculated using the method above results in a mass a factor of 8 lower than that determined by Benson & Myers (1989) for the same core. Using the above definitions, we find better agreement between M_n and M_N for the cores mapped here, and also for many cores in other complexes.

The masses are listed in Table 3, along with errors propagated from the errors in r, n, and N. The errors in M_N are typically larger than the errors in M_n due to the greater uncertainty in N, but the errors in M_n do not reflect the uncertainty which arises from assuming that the line-of-sight size of these clumps is similar to their map size r.

The cores of the "new Perseus sample" (hereafter NPS) have remarkably similar properties. The mean intrinsic NH_3 line width of the group is 0.35 km s^{-1}, with a standard deviation of only 0.05 km s^{-1}, which is nearly as small as the uncertainty of each measurement. Similarly, the mean kinetic temperature is 11 K, with a standard deviation of 0.4 K, which is much less than the uncertainty in the individual temperatures. The derived volume densities n all have log $n \sim 4$, with the exception of Per 5. Toward Per 5, we have found a high value for the volume density (log $n = 5.0$), mainly because the source is bright ($T_A^* \sim 0.8$ K) and very compact. However, our estimate for the filling factor in our 88″ beam (0.52) is not well constrained by the map, and even small errors in this value will affect the volume density estimate. If the filling factor is instead as large as 0.7, the derived volume density drops to 3×10^4 cm^{-3}, which is more similar to the values derived toward other cores in this sample.

The mean value of r in individual clumps is 0.11 pc (standard deviation $\sigma = 0.03$ pc), while the value for complexes (i.e., considering adjoining clumps together) is 0.13 pc ($\sigma = 0.04$ pc). The average value for M_n in individual clumps is 5 $M_\odot$ ($\sigma = 4$

TABLE 3

NH_3 CORE PARAMETERS

Name	r (pc)	log n (cm^{-3})	log N_{H_2}[a] (cm^{-2})	M_n ($M_\odot$)	M_N ($M_\odot$)
Observations Reported in This Paper					
Per 1	0.12(4)	...	...	...	...
Per 3	0.15(1)	4.2	22.1	12(2)	11(22)
Per 4	0.21(3)	4.0	22.0	19(8)	16(36)
N clump	0.14(3)	4.0	22.0	6(4)	7(17)
S clump	0.17(2)	4.0	22.0	12(4)	11(25)
Per 5	0.07(1)	5.0	22	6(3)	2(4)
Per 6	0.11(1)	4.3	22	5(1)	4(9)
Per 7	0.16(2)	3.9	22.0	8(3)	10(22)
E clump	0.09(2)	4.1	22.1	2(1)	4(6)
W clump	0.11(2)	3.7	22.0	1(1)	4(9)
Per 9	0.09(2)	4.1	22.2	2(1)	5(6)
E clump	0.12(4)	4.1	22.2	1(1)	3(3)
W clump	0.07(2)	4.1	22.2	5(5)	8(9)
Observations Reported Previously					
L1448[b]	0.21	4.5	22.5	61	49
L1455[b]	0.26	4.0	22.0	38	24
N clump	0.15	4.0	22.0	8	8
C clump	0.16	4.0	22.0	10	10
S clump	0.15	4.0	22.0	8	8
NGC 1333[c]	0.29	4.3	22.5	106	97
HH 7–11	0.17	4.3	22.5	23	35
HH 12	0.12	4.3	22.5	7	16
I03282[d]	0.07	4.8	22.3	5	4
B1[e]	0.24	4.0	22.0	17	8
IC 348[f]	0.18	4.0	21.4	12	9
E clump	0.09	4.2	21.4	3	3
N clump	0.10	4.5	21.4	8	3
S clump	0.05	4.0	21.4	0.3	0.7
B5[g]	0.19	3.8	21.5	9	4
N clump	0.11	3.8	21.5	1.7	1.3
S clump	0.12	3.8	21.5	2.3	1.6

NOTE.—No estimates for n and N (and hence M_n and M_N) are available for Per 1 due to the low quality of the $(J, K) = (1, 1)$ spectrum and the lack of a (2, 2) spectrum.

[a] N_{H_2} is determined from N_{NH_3}, assuming an abundance of NH_3 relative to H_2 of 10^{-7}.

[b] Anglada et al. 1989.

[c] Ho & Barrett 1980.

[d] Bachiller et al. 1991.

[e] Bachiller et al. 1990a.

[f] Bachiller et al. 1987.

[g] Benson & Myers 1989.

TABLE 4

MEAN VALUES OF NH_3 CORE SAMPLES

Sample	No. of Cores	$\overline{\Delta V}$ (km s^{-1})	$\bar{T}_K$ (K)	$\bar{r}$ (pc)	$\bar{M}_N$ ($M_\odot$)	$\bar{M}_n$ ($M_\odot$)
New Perseus sample (NPS)	10	0.35(0.05)	11(0.4)	0.11(0.03)	6(3)	5(4)
Combined Perseus sample (CPS)	22	0.55(0.32)	13(3)	0.12(0.04)	9(13)	9(12)
Taurus sample	12	0.33(0.1)	10(2)	0.06(0.01)	1.1(0.7)	1.2(1.3)
Orion sample	17	1.12(0.5)	17(4)	0.15(0.07)	21(25)	...[a]

NOTE.—Numbers in parentheses are the 1 σ dispersions in each sample about the listed mean value.

[a] Mean value of M_n is not listed for the Orion sample because estimates of n are not available for many of the cores in this sample.

$M_\odot$), while the average value for M_N is 6 $M_\odot$ ($\sigma = 3\ M_\odot$). The average value for M_n in complexes is 8 $M_\odot$ ($\sigma = 5\ M_\odot$), while the average value for M_N is 7 $M_\odot$ ($\sigma = 4\ M_\odot$). In all cores, M_n and M_N differ by less than the errors on M_N. The mean properties for the individual clumps in the NPS are tabulated in Table 4.

3.3. *Comparison with Other Cores in Perseus*

From the literature, we compiled a list of sources in Perseus previously observed in NH_3, and we list the properties of those cores with the properties of our new cores in Table 3. We have determined r in the same manner for these cores that was used in equation (1), and we adopt the published estimates for n and N_{H_2}. M_n and M_N are calculated as in equations (2) and (3), respectively. Emission from four of the six previously observed regions can be divided into clumps, based on examination of the published maps. We have calculated r, M_n, and M_N for these clumps as well. Combining these cores with the NPS, we construct the "combined Perseus sample" (hereafter CPS) of 23 individual clumps of NH_3 emission and list the mean properties of this sample in Table 4.

Most of the mean properties of the CPS are quite similar to, but slightly greater than, the mean properties of the NPS. The mean values of r and T_K are only about 10% larger. However, the mean line width of the CPS is nearly a factor of 2 greater than the mean line width of the NPS. Thus it appears that the cores studied previously are more turbulent than the NPS.

The average value of M_n for individual clumps in the CPS is 9 $M_\odot$ ($\sigma = 12\ M_\odot$), and the average value of M_N is 9 $M_\odot$ ($\sigma = 13\ M_\odot$), suggesting that the cores in the NPS are less massive than the previously mapped cores. Four out of 13 of the previously studied clumps are more massive than any core in the NPS. Furthermore, the mean complex mass of the previously studied cores is much higher ($\bar{M}_N = 28\ M_\odot$) than the mean complex mass of the NPS ($\bar{M}_N = 8\ M_\odot$), indicating that the cores in the NPS represent the lower mass and more isolated component of the CPS.

3.4. *Comparison with Cores in Other Complexes*

In addition to Perseus, two other molecular cloud complexes, Taurus and Orion A, have been studied in the NH_3 line in similar detail. In this section, we use the same methodology to compare the properties derived from the CPS with the properties of cores in these other complexes, using data from the literature.

It is particularly useful to compare the CPS with cores from these two cloud complexes, because these complexes are so different from one another in terms of their star formation output. The Taurus complex generally produces stars of low luminosity and final stellar mass, mostly in small isolated groups with low surface density (Jones & Herbig 1979; Gomez et al. 1993). In contrast, the Orion complex produces stars of much higher mass and luminosity, and much of the star formation is more clustered into a few sites of vigorous activity (e.g., McCaughrean 1989).

We have chosen cores in Taurus from the lists of Benson & Myers (1989), Menten & Walmsley (1985), and Ungerechts, Walmsley, & Winnewisser (1982). Since our survey was based on a source list derived from the *IRAS* PSC, we have selected only those cores associated with *IRAS* sources. We found 10 such sources in Benson & Myers (1989) and added the cores associated with IRAS 04287+1801 (Menten & Walmsley 1985) and IRAS 04325+2702 (Ungerechts et al. 1982), both of which are also associated with *IRAS* PSC sources.

The mean properties of this sample of NH_3 cores in Taurus are listed in Table 4, along with the standard deviation in each mean value. It is quite clear from these values that the Taurus sample differs quite considerably from the CPS, particularly in terms of line width and size. The mean line width of the CPS is larger than the line widths of all but one Taurus core. The mean value for r in the Taurus sample is 0.06 pc—about one-half the value for the CPS. The mean value for M_n is 1.2 $M_\odot$ ($\sigma = 1.3\ M_\odot$), and the mean value of M_N is 1.1 $M_\odot$ ($\sigma = 0.7\ M_\odot$). Both mass mean values are considerably smaller than those found in the CPS.

To construct a sample of cores in the Orion A complex, we have used the NH_3 survey of Wouterloot et al. (1988) to identify NH_3 emission associated with *IRAS* PSC sources. Twelve cores satisfy these criteria, 10 of which have been mapped by Wouterloot et al. (1988) and Harju et al. (1991). From the two sources that were not mapped, we can obtain measurements of ΔV and T_K, but we have no information about the size or mass of these cores.

We have also added those cores mapped by Batrla et al. (1983) and Cesaroni & Wilson (1994) along the ridge of dense gas near the Orion A H II region. All these cores are likely associated with young stars due to the high density of sources in this region; however, we will choose only those five cores clearly associated with *IRAS* PSC sources to add to our sample. These five cores have properties that are representative of the variety of conditions in all the cores along the ridge. Thus our Orion sample contains 17 cores, 15 of which have been mapped.

The mean properties of the Orion sample are listed in Table 4, along with the standard deviation in each mean value. A comparison of these mean values with the mean values from the CPS shows that the Orion sample also differs quite considerably from the CPS, but unlike, the values for the Taurus sample, the Orion mean values are all larger than the CPS mean values. In particular, the mean mass ($\bar{M}_N$) and line width

are more that twice as large as the CPS mean values, while the mean size and kinetic temperature are larger by factors between 1 and 2.

Histograms of these properties for the three complexes show even more clearly how Perseus appears to be intermediate between Orion and Taurus in its dense core properties. Figures 9, 10, 11, and 12 show histograms of line width, size, kinetic temperature, and mass M_N for the three complexes.

Figure 9 is indicative of the differences between the NH_3 cores in the three complexes, as well as their relative ranking. In the Taurus sample, most of the cores have line widths less than 0.32 km s^{-1}, while most of the cores in CPS have line widths between 0.32 km s^{-1} and 1 km s^{-1}, and in Orion, almost half have line widths greater than 1 km s^{-1}. We assess the significance of the differences between these distributions using the Kolmogorov-Smirnov (K-S) test. The probability that the Taurus and CPS samples have been drawn from the same parent sample is 2×10^{-3}, while the probability that the Perseus and Orion samples have been drawn from the same parent distribution is 10^{-5}. These results indicate that all three samples are probably drawn from separate parent distributions, but that the CPS is more similar to the Taurus sample in line width.

However, the CPS looks much more like the Orion sample than the Taurus sample in terms of core radius (Fig. 10). Both in terms of the peaks of the distributions at 0.1 pc and the tails toward large size, the CPS is strikingly similar to the Orion sample. In contrast, the Taurus sample is much more centrally peaked at 0.06 pc and has no tail toward large sizes. The K-S test indicates that the CPS and Orion samples are not significantly different (the probability that they come from the same parent sample is 2×10^{-2}) but that the Taurus and CPS samples are quite significantly different, with a probability that they come from the same parent sample of 10^{-6}.

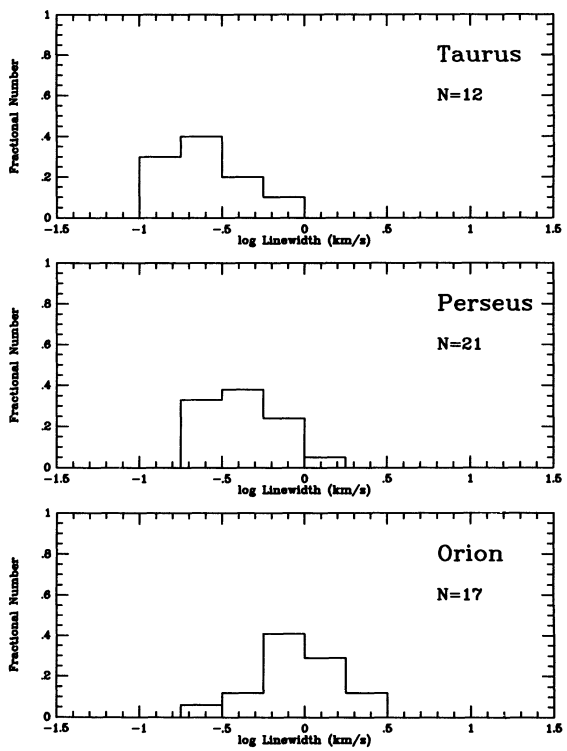

FIG. 9.—Histogram of core NH_3 line width for the Taurus sample (*top*), the CPS (*middle*), and the Orion sample (*bottom*). Note that all three plots are normalized. The number of cores used in each sample is indicated at right.

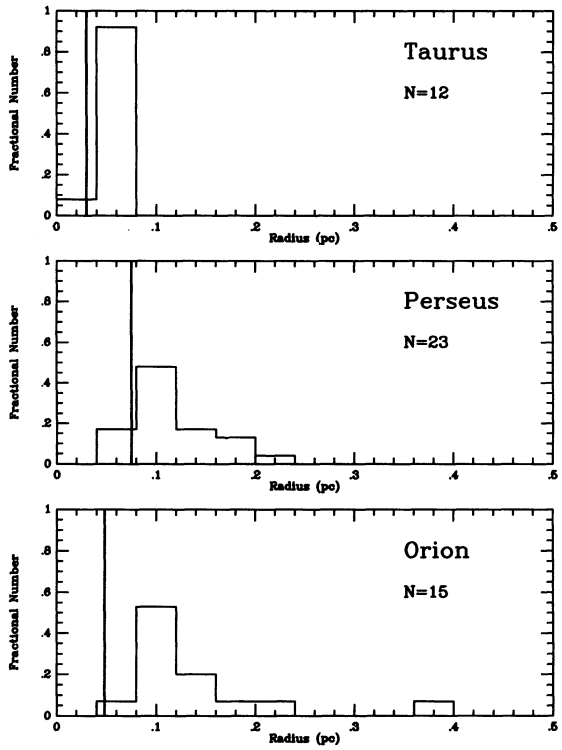

FIG. 10.—Histogram of core size for the Taurus sample (*top*), the CPS (*middle*), and the Orion sample (*bottom*). Note that all three plots are normalized. The number of cores used in each sample is indicated at right.

The radius of the largest beam size used to observe the cores in each of the samples is indicated in the panels of Figure 10 by a heavy vertical line (some of the cores in the Taurus and Perseus samples have been observed with smaller beam sizes). While the size of each core has already been corrected for the telescope beam, it is telling to note that in all three samples, the peak of the histogram occurs in the bin just larger than the telescope beam size. This suggests that in all three regions, some of the cores may be underresolved. However, the existence of large-size tails in the histograms of the Orion and Perseus samples still distinguishes them from the Taurus sample.

The kinetic temperature histogram of the CPS, shown in Figure 11, is fairly distinct from both the Taurus and Orion histograms. All three samples appear to be significantly different, based on K-S statistics. Like the Taurus sample, the CPS is quite centrally peaked, but the CPS distribution peaks at a higher temperature than the Taurus distribution. The Orion sample is distributed over a much larger range in kinetic temperature, from 9 to 27 K.

Only in the mass distribution does the CPS show considerable breadth (Fig. 12). Here while the Taurus and Orion samples appear to be more centrally peaked, the Perseus distribution is more smoothly distributed from about 1 $M_\odot$ to about 30 $M_\odot$. In contrast, most of the cores in the Taurus sample have M_N less than 1 $M_\odot$, and the Orion sample peaks sharply at about 15 $M_\odot$. The probability that any two of these samples was drawn from the same parent is less than 5×10^{-5}. Note that if some of the Perseus cores are underresolved by the

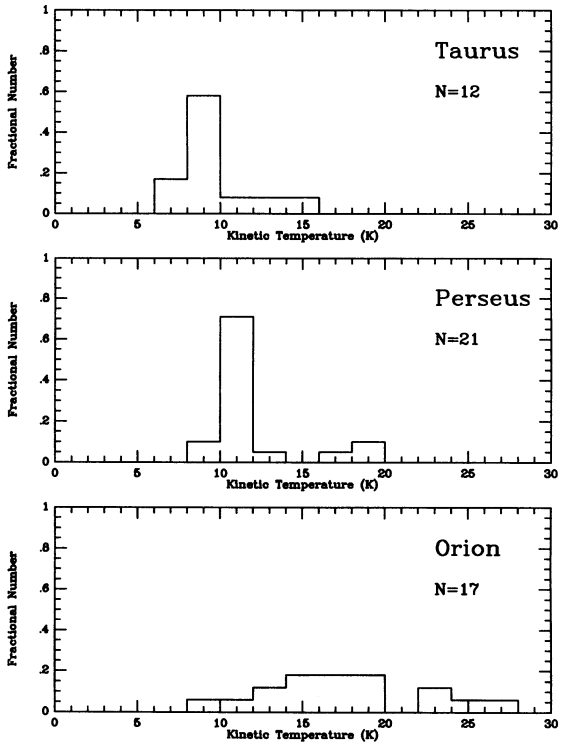

FIG. 11.—Histogram of core kinetic temperature for the Taurus sample (*top*), the CPS (*middle*), and the Orion sample (*bottom*). Note that all three plots are normalized. The number of cores used in each sample is indicated at right.

telescope beam (see above), then the masses derived are upper limits to the true mass. This effect would only further broaden the CPS mass histogram and make it even more significantly different from the Taurus and Orion samples.

Using the kinetic temperatures and line widths derived from these data, we can compare the thermal and nonthermal energy content of each of the cores. We calculate the thermal line width, ΔV_T, as

$$\Delta V_T^2 = 8 \ln 2 \frac{kT_k}{2.3\ m_p}, \tag{4}$$

and the nonthermal line width, $\Delta V_{\rm NT}$, as

$$\Delta V_{\rm NT}^2 = \Delta V^2 - 8 \ln 2 \frac{kT_k}{m_0}, \tag{5}$$

where T_K is the kinetic temperature derived from the data, ΔV is the intrinsic NH_3 line width, k is Boltzmann's constant, m_p is the mass of a proton, and m_0 is the mass of the NH_3 molecule. This method is exactly the same as that used by Myers et al. (1991).

Histograms of the ratio of nonthermal to thermal energy for all three samples are shown in Figure 13. In both the CPS and the Taurus sample, the majority of the cores are thermally dominated; i.e., their thermal line width exceeds their nonthermal line width. Only two cores in the Taurus sample and six cores in the CPS have energy ratios greater than unity. In contrast, most of the cores in the Orion sample are nonthermally dominated, and in some cases the nonthermal energy exceeds 10 times the thermal energy content. The prob-

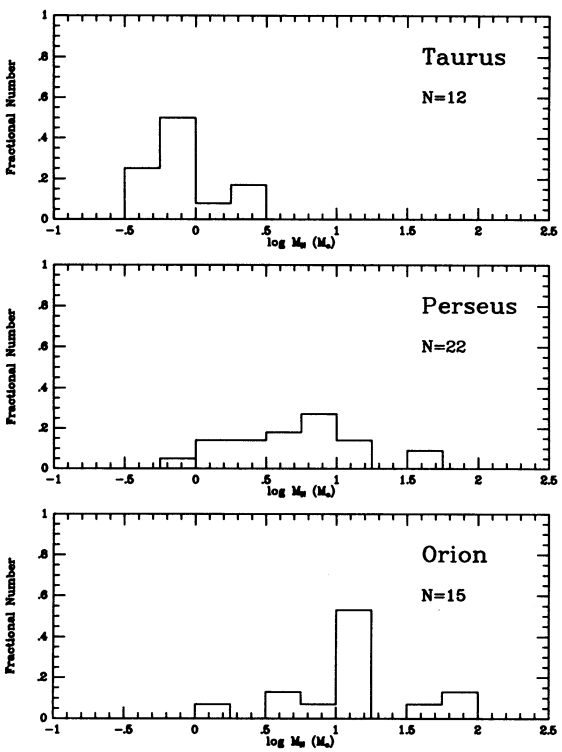

FIG. 12.—Histogram of core mass (M_N) for the Taurus sample (*top*), the CPS (*middle*), and the Orion sample (*bottom*). Note that all three plots are normalized. The number of cores used in each sample is indicated at right.

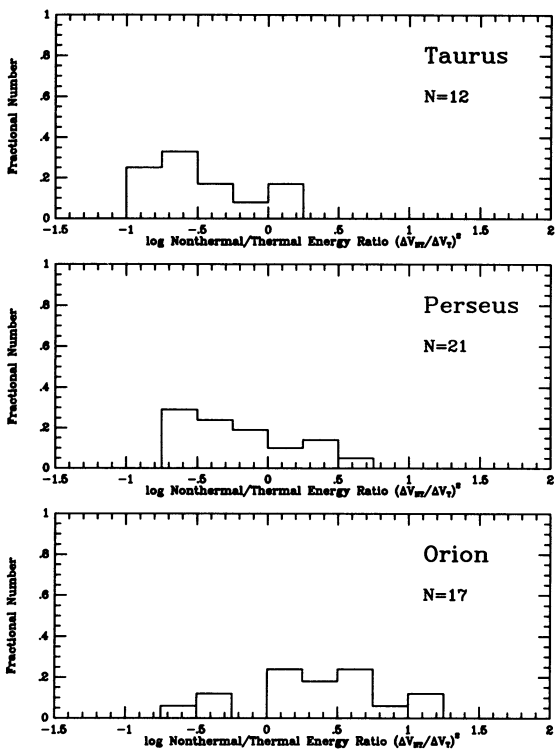

FIG. 13.—Histogram of the thermal/nonthermal energy ratio for the Taurus sample (*top*), the CPS (*middle*), and the Orion sample (*bottom*). Note that all three plots are normalized. The number of cores used in each sample is indicated at right.

ability that the CPS and the Taurus sample were drawn from the same parent distribution is 5×10^{-3}, indicating that the differences between them are probably only marginally significant. However, the probability that the CPS and Orion samples were drawn from the same parent distribution is 4×10^{-5}, and we conclude that these distributions are significantly different.

Thus, while the mean properties of the three complexes suggest that Perseus is intermediate between Taurus and Orion in its dense core properties, the histograms demonstrate that some of the properties of the CPS are more like those of the Taurus sample, while the others are more like those of the Orion sample. The distributions suggest that while Perseus is indeed intermediate in its dense gas properties between Taurus and Orion, it is more appropriately labeled "hybrid" in that the CPS contains elements similar to both the Taurus and Orion samples. Nowhere is this distinction clearer than in the distribution of masses in the three samples. While the Taurus and Orion samples are fairly centrally peaked at very different masses, the CPS is much more broadly distributed, spanning the gap between the Taurus and Orion distributions.

However, it does not appear that Perseus is simply a mixture of low-mass cores like those in Taurus and high-mass cores like those in Orion. The cores in Perseus with line widths similar to those in the Taurus sample have larger sizes, higher masses, and slightly higher kinetic temperatures than their Taurus counterparts. Likewise, the Perseus cores with sizes similar to those in the Orion sample have lower kinetic temperatures and narrower line widths than their Orion counterparts.

4. DISCUSSION

4.1. *Star Formation within Perseus*

Our new observations show that, in addition to the dense gas associated with the well-known clusters and more luminous sources in Perseus, there are many thermally dominated cores associated with less luminous and more isolated sources in the complex. The NPS cores are typically much less massive than the ones previously observed toward NGC 1333, B1, and L1448, and together they account for less than 25% of the total detected dense gas mass in the complex. In fact, the total mass of all of the NPS cores is approximately half of the mass contained in dense gas toward NGC 1333.

4.1.1. *Spatial Distribution*

These cores show that the spatial distribution of dense gas in Perseus is not confined to the well-known centers of current and recent star formation. The previous observations concentrated on strong column density peaks in the complex, while the new detections presented here are found throughout the complex, at the positions of smaller column density peaks (see Fig. 1). These new observations add an isolated low-mass component to the distribution of dense gas in the complex.

The spatial distribution of dense cores is not random, however. Four new cores (Per 3, two toward Per 4, and Per 5) are located near the NGC 1333 core, and four others (two each toward Per 7 and Per 9) are located near B1. Toward both B1 and NGC 1333, the cores are roughly aligned along a north-northeast–south-southwest axis.

Figure 14 shows the distribution of the NH_3 cores in the NGC 1333 region, along with all the *IRAS* PSC sources, including the sources detected by the pointed *IRAS* study of NGC 1333 by Jennings et al. (1987). The dense gas in this region appears to be organized into a "ridge" extending $\sim 20'$ (~ 2 pc) to the north-northeast and south-southwest of NGC 1333. The projected separation between individual cores is about 0.5 pc along the ridge, and may be smaller since the ridge has not been fully sampled in NH_3. (Benson 1992 reports detecting NH_3 emission at the position of the embedded infrared source SVS-3, which is located at [6.2, 0.6] in Fig. 14, and another core has been detected toward an extinction peak at [−7.1, −3.6]; Ladd, Myers, & Goodman 1994). The infrared sources also appear to be preferentially located along the ridge and, in particular, clustered toward NGC 1333. In the near-infrared, the clustering toward NGC 1333 is even more prominent, with over 100 sources detected within a $6' \times 6'$ region (Aspin & Sandell 1991).

An emission structure of similar extent and position angle can be seen in the CO and ^{13}CO $J = (1 \rightarrow 0)$ maps of Loren (1976), although Loren's maps show less emission to the north of NGC 1333 toward Per 4 and Per 5. The ridge can also be seen in the larger beam size and slightly undersampled ^{13}CO $J = (1 \rightarrow 0)$ map of Bachiller & Cernicharo (1986; Fig. 1),

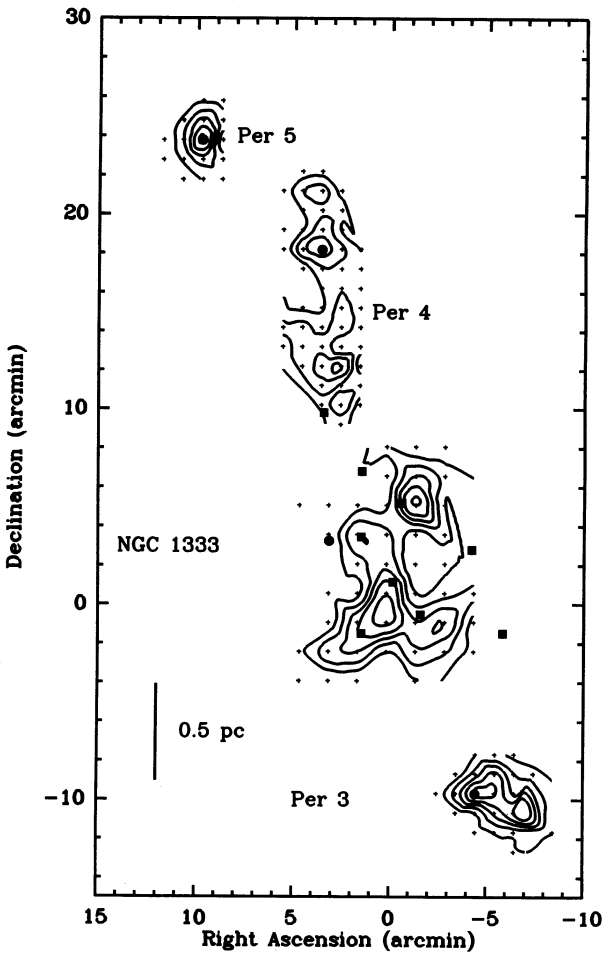

FIG. 14.—Contours of T_A^* toward the NGC 1333 ridge. The data for cores Per 3, Per 4, and Per 5 are from this work; the data for NGC 1333 are from Ho & Barrett (1980) and have been multiplied by 1.5 to account for the improvement in the efficiency of the Haystack antenna between 1980 and 1991. Contours start at 0.15 K and increment by 0.15 K. Filled squares mark the positions of *IRAS* sources detected by Jennings et al. (1987) in their pointed study. Filled squares mark the positions of *IRAS* PSC sources outside the field of view of the Jennings et al. observations.

although its half-power extent is also smaller than the full extent of the ridge seen in NH_3. It is quite likely that because of high column densities in this region, these CO maps are more sensitive to temperature than column density and therefore peak more strongly at the position of NGC 1333. However, it is also clear that these NH_3 cores are the densest part of a connected structure of high column density extending over ~ 4 pc.

Another less massive ridge structure can be seen in the Perseus complex near B1 (Fig. 15). Here new cores Per 6, Per 7, and Per 9 align with previously observed cores B1 (Bachiller et al. 1990a) and I03282 (Bachiller et al. 1991) along a northeast–south-southwest axis extending over slightly more than 1° (~ 6 pc). The *IRAS* sources in this region also appear to be distributed along the same axis. The projected separation between NH_3 is larger than the projected separation between cores in the NGC 1333 ridge, though this ridge is not as well sampled in NH_3. The northernmost three NH_3 cores are within a curving ridge of high column density material measured in $C^{18}O$ $J = (1 \rightarrow 0)$ and CS $J = (1 \rightarrow 0)$ emission (Bachiller et al. 1990a). These NH_3 cores are coincident with three of four CS peaks identified by Bachiller et al. (1990a).

4.1.2. *Association with Young Stars*

The *IRAS* sources associated with the cores of the NPS are of lower luminosity than the sources associated with the previously observed cores in Perseus. Many of these sources have only been detected in one band in the PSC. However, all these *IRAS* source positions have been searched at 2 μm, and near-infrared counterparts to six out of the eight *IRAS* sources have been found, including four out of five sources detected in only one band by *IRAS* (Ladd 1991; Ladd et al. 1993). Combining the near-infrared photometry with the *IRAS* PSC detections or ADDSCAN fluxes where available (Clark 1991), we find that the mean luminosity of the sources associated with the cores of the NPS is $\bar{L} = 1.0\, L_\odot$ ($\sigma = 0.7\, L_\odot$).

These sources also appear to be single and relatively isolated. The near-infrared survey of these sources mapped out the *IRAS* error beam and, with one exception, found at most one near-infrared source in each field to a detection limit of 16.5 mag at K (toward IRAS 03380+3135 two sources were found). Therefore we conclude that the sources associated with the cores of the NPS are not members of clusters or stellar density enhancements of the type seen toward NGC 1333 and IC 348 in the Perseus complex, or toward many of the red *IRAS* sources in the Orion A complex (Chen & Tokunaga 1994). However, because of the field of view (45″) and pixel scale (0″.8) of the infrared survey, we cannot rule out less concentrated clusters or binary systems with separations $\lesssim 1$.

In addition to being associated with lower luminosity sources, the cores of the NPS also have the smallest and most thermally dominated line widths of all the cores in the Perseus complex. We plot the thermal and nonthermal line widths for all the Perseus cores as a function of luminosity in Figure 16. For each multiple-peaked region in Table 3, we choose only the core closest to the luminosity source for display, so only 14 pairs of points are plotted. The correspondence between both thermal and nonthermal line width and luminosity is evident in this plot. This relation was first noted by Myers et al. (1991) when comparing a large number of cores from many different complexes, but here we find that the trend is present even for cores taken from a single complex. Myers et al. (1991) found that the division between thermally dominated and nonthermally dominated cores occurs at a luminosity of about 10 $L_\odot$; our Perseus data also appear consistent with that finding, although the number of cores containing sources of luminosity $> 10\, L_\odot$ is very small.

The data presented here indicate that the dense gas in the Perseus complex exists under a wide variety of conditions, ranging from relatively quiescent, isolated low-mass cores in the environs of low-luminosity objects, to massive, highly turbulent cores located within rich young clusters. This conclusion is similar to the result found by Ladd et al. (1993), who note in their infrared study of the complex that star formation takes place in both spatially isolated and clustered modes within the complex.

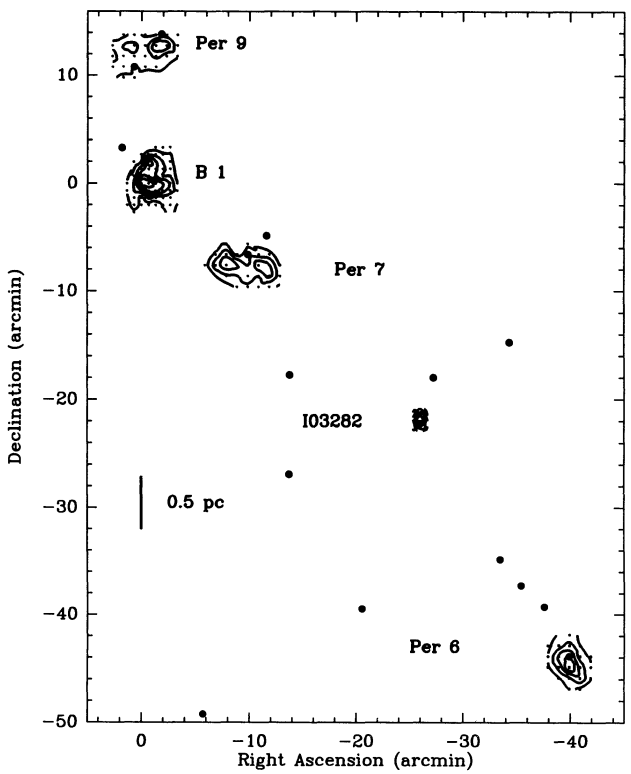

FIG. 15.—Contours of T_A^* toward the B1 region. The data for cores Per 7 and Per 9 are from this work; the data for B1 and IRAS 03282 have been estimated by eye from the integrated NH_3 intensity maps of Bachiller et al. (1990a, 1991). The scaling of the B1 and IRAS 03282 data relative to Per 6, Per 7, and Per 9 is arbitrary for this schematic. Contours for the Per 7 and Per 9 data start at 0.1 K and increment by 0.1 K. Filled circles mark the positions of *IRAS* PSC sources.

4.2. *Perseus in Relation to Taurus and Orion*

The NH_3 results presented here, along with the infrared results presented by Ladd et al. (1993) indicate that the Perseus complex is intermediate in its star-forming properties between the regions like Taurus, which produce mainly low-luminosity stars, and those regions like Orion, which are capable of producing stars of much higher mass. The mean mass of the Perseus NH_3 cores is significantly greater than the mean mass of the NH_3 cores in Taurus, and somewhat less than the mean mass in L1641. The average values for the thermal and nonthermal line widths in these cores are also intermediate between the predominantly thermally dominated cores in

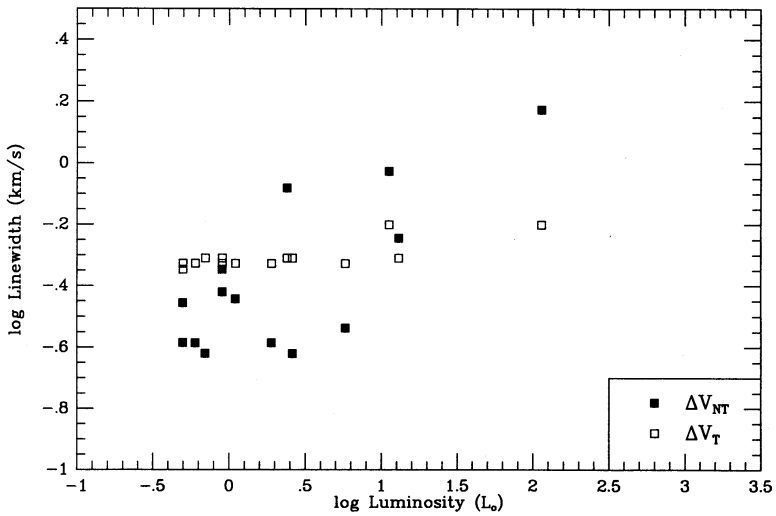

FIG. 16.—Thermal and nonthermal line width vs. luminosity for the Perseus cores with associated luminosity sources. Nonthermal line width is indicated by the filled squares, and thermal line width is indicated by the open squares.

Taurus and the predominantly nonthermally dominated cores in L1641.

The organization of the dense gas within the complex is also an indicator that Perseus is intermediate between Taurus and Orion. Many of the known dense cores in Perseus are aligned within two large filamentary structures, much like the long linear NH_3 structure seen connecting OMC-1 and OMC-2 (Cesaroni & Wilson 1994). However, the largest ridge in Perseus (the NGC 1333 ridge) is roughly a factor of 2 less massive and smaller in linear extent than the Orion ridge, and in NH_3, it does not appear to be as well connected or organized into a single linear element. Filamentary structure is also seen in Taurus, but usually with a lower volume density tracer (e.g., ^{13}CO, Fukui et al. 1991; H_2CO, Clark 1991). All three complexes show filamentary structure, but in Taurus, the filaments may rarely have densities high enough to excite NH_3 emission, while in Orion, the filament densities are high enough to excite NH_3 emission all along their length. Filaments in Perseus may have densities high enough to excite NH_3 emission only at some places along the filament's length. Thus in Orion, the NH_3 cores are almost continuously connected, and in Perseus the cores are aligned but not connected. With perhaps only one NH_3 core per filament in Taurus, the distribution of NH_3 cores shows no linear organization.

The relationship between the cores and their associated sources also indicates that Perseus occupies the middle ground between Taurus and Orion. In Figure 17, we plot the thermal and nonthermal line widths of the cores in all three complexes as a function of the luminosity of their associated stars. The upward trend in thermal line width, nonthermal line width, and the ratio between nonthermal and thermal line width as a function of luminosity is more evident in this plot than in Figure 16, not because of any increase in dynamic range in luminosity or line width, but rather because of the addition of two nearly segregated samples—the low-luminosity, thermally dominated cores of the Taurus sample and the high-luminosity, nonthermally dominated cores of the Orion sample. While the Taurus and Orion samples are segregated

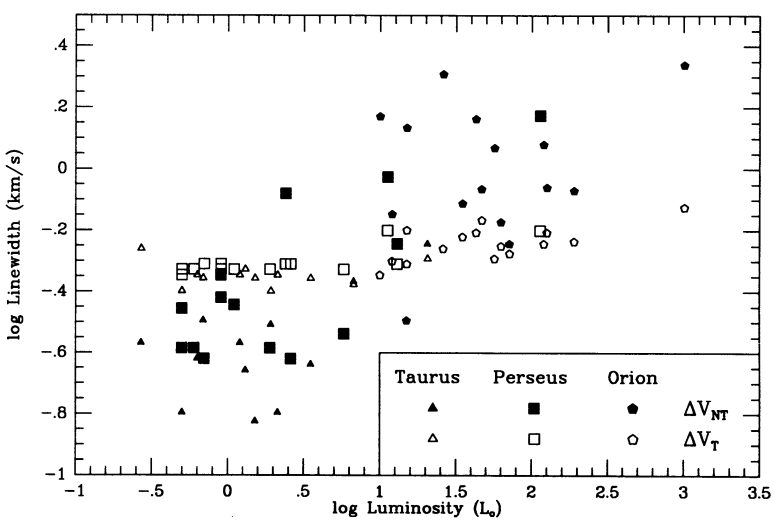

FIG. 17.—Thermal and nonthermal line width vs. luminosity for the Taurus, Perseus, and Orion cores with associated luminosity sources. Nonthermal line width is indicated by the filled symbols, and thermal line width is indicated by the open symbols.

into the thermal and nonthermal regions of the diagram, the cores of the Perseus sample span the entire dynamic range.

Although the mean properties suggest that Perseus occupies an intermediate state between these two extreme modes of star-forming clouds, it is perhaps more accurate to describe Perseus as a hybrid combination of the two. In its isolated population, Perseus appears to be much more like Taurus, with single stars of low luminosity forming from individual, thermally dominated NH_3 cores. However, its more massive cores harbor young stars of higher luminosity that form in groups or clusters much like the cores in L1641. Furthermore, the most massive core in Perseus, in NGC 1333, is associated with a rich cluster of more than 100 young stars (Aspin & Sandell 1991).

A rank-ordering of the star-forming capability of molecular clouds has been sought by several authors. Myers (1991) suggested that clouds might be ordered by their gravitational potential, in which clouds with high masses and densities preferentially produce more stars of higher mass in more clustered environments. Wiseman & Adams (1994) have ordered nearby clouds based on their structure derived from maps of 60 μm and 100 μm continuum emission. They define a cloud's "complexity" based on measures of the fraction of cloud material at high column density, the number of filaments, and gravitational potential, and note that more complex clouds appear to harbor more vigorous star formation activity.

The common trend in core and young star properties seen in the three clouds examined here supports the hypothesis that the large-scale properties of a molecular cloud influence the type of star formation within and, furthermore, that more massive, more turbulent molecular clouds contain larger, more nonthermally dominated dense cores, which in turn produce more massive stars and richer clusters.

5. CONCLUSIONS

1. We have surveyed 10 positions in the Perseus molecular cloud complex for 23 GHz NH_3 line emission and detected NH_3 in eight positions. At seven of these positions, we have constructed maps of NH_3 dense cores, bringing the total number of mapped regions of NH_3 emission in Perseus to 14. These new cores have a mean kinetic temperature of 11 K, mean size of 0.11 pc, mean line width of 0.35 km s^{-1}, and mean mass of 6 $M_\odot$. All these means are smaller than those derived from the cores previously studied in Perseus.

2. The NH_3 cores in Perseus as a group have a mean size of 0.12 pc, mean line width of 0.6 km s^{-1}, mean kinetic temperature of 13 K, and mean mass of 9 $M_\odot$. The mean values are larger than the mean values for cores associated with young stars in the Taurus complex, but smaller than the mean values of cores associated with young stars in the Orion A complex. Histograms of these quantities suggest that the Perseus cores are similar to Taurus cores in their line width and kinetic temperature, while they are more similar to Orion cores in their size. The mass distribution of the Perseus cores is intermediate between the mass distributions of the Taurus and Orion cores.

3. Many of the detected NH_3 cores in Perseus are located along two high-density ridges, one centered on the NGC 1333 region and another extending southwest from the B1 core. These ridges are 4–6 pc in extent and contain over 60% of the dense gas mass detected in Perseus.

4. We partition the observed line width into thermal and nonthermal components and find that many of the Perseus cores are thermally dominated, but a significant fraction (6 of 21) are dominated by nonthermal motions. This property distinguishes Perseus from Taurus, where nearly all the NH_3 cores are dominated by thermal motions (10 of 12), and Orion, where nearly all the NH_3 cores are dominated by nonthermal motions (14 of 17). Furthermore, a plot of line width versus luminosity shows that, while the Taurus cores are preferentially located in a low-luminosity, thermally dominated regime and the Orion cores are preferentially located in a high-luminosity, nonthermally dominated regime, the Perseus cores span the entire range in luminosity and line width.

5. The mean properties of the Perseus sample of NH_3 cores identify Perseus as an intermediate complex between Taurus, whose cores are less massive and more quiescent and have produced stars of lower luminosity, and Orion A, whose cores are more massive and more turbulent and have produced stars of higher luminosity. We conclude that Perseus is a hybrid complex, containing examples of isolated, low-mass star formation, as well as examples more commonly associated with higher mass, clustered star formation.

The authors thank M. Forbes for assistance in obtaining the NH_3 data, G. Fuller for a careful reading of the manuscript, and the staff of the Haystack Observatory for their support in the data acquisition. We also thank P. Benson for providing her NH_3 line-fitting program. E. F. L. acknowledges support from the James Clerk Maxwell Telescope Fellowship.

REFERENCES

Anglada, G., Rodriguez, L. F., Torrelles, J. M., Estalella, R., Ho, P. T. P., Canto, J., Lopes, R., & Verdes-Montenegro, L. 1989, ApJ, 341, 208
Aspin, C., & Sandell, G. 1991, JCMT-UKIRT Newsletter, 1, 21
Bachiller, R., & Cernicharo, J. 1986, A&A, 166, 283
Bachiller, R., Cernicharo, J., Martin-Pintado, J., Tafalla, M., & Lazareff, B. 1990a, A&A, 166, 283
Bachiller, R., Guilloteau, S., & Kahane, C. 1987, A&A, 173, 324
Bachiller, R., Martin-Pintado, J., & Planesas, P. 1991, A&A, 251, 639
Bachiller, R., Menten, K. M., & del Rio-Alvarez, S. 1990b, A&A, 236, 461
Bally, J. 1991, private communication
Batrla, W., Wilson, T. L., Bastien, P., & Ruf, K. 1983, A&A, 128, 279
Benson, P. J. 1983, Ph.D. thesis, MIT
———. 1992, private communication
Benson, P. J., & Myers, P. C. 1989, ApJS, 71, 89
Blaauw, A. 1952, Bull. Astron. Inst. Netherlands, 11, 405
Borgman, J., & Blaauw, A. 1964, Bull. Astron. Inst. Netherlands, 17, 358
Cernichaaro, J., & Bachiller, R. 1984, A&AS, 58, 327
Cernicharo, J., Bachiller, R., & Duvert, G. 1985, A&A, 149, 273
Cesaroni, R., & Wilson, T. L. 1994, A&A, 281, 209
Chen, H., & Tokunaga, A. T. 1994, ApJS, 90, 149
Clark, F. O. 1991, ApJS, 75, 611
Cohen, M., & Kuhi, L. V. 1979, ApJS, 41, 743
Davidson, J. A., & Jaffe, D. J. 1984, ApJ, 277, L13
Fukui, Y., Mizuno, A., Nagahama, T., Imaoka, K., & Ogawa, H. 1991, Mem. Soc. Astron. Ital., 62, 801
Fuller, G. A., Myers, P. C., Welch, W. J., Goldsmith, P. F., Langer, W. D., Campbell, B. G., Guilloteau, S., & Wilson, R. W. 1991, ApJ, 376, 135
Goldsmith, P. F., Langer, W. D., & Wilson, R. W. 1986, ApJ, 303, L11
Goldsmith, P. F., Snell, R. L., Hemeon-Heyer, M., & Langer, W. D. 1984, ApJ, 286, 599
Gomez, M., Hartmann, L., Kenyon, S. J., & Hewett, R. 1993, AJ, 105, 1927
Goodman, A. A., Crutcher, R. M., Heiles, C., Myers, P. C., & Troland, T. H. 1989, ApJ, 388, L61
Harju, J., Walmsley, C. M., & Wouterloot, J. G. A. 1991, A&A, 245, 643
Harris, D. L., Morgan, W. W., & Roman, N. G. 1954, ApJ, 119, 622
Harvey, P. M., Wilking, B. A., & Joy, M. 1984, ApJ, 278, 156
Herbig, G. H., & Bell, K. R. 1988, Lick Obs. Bull. No. 1111
Herbig, G. H., & Jones, B. F. 1983, AJ, 88, 1040
Heyer, M. H., Snell, R. L., Goldsmith, P. F., Strom, S. E., & Strom, K. M. 1986, ApJ, 308, 134
Ho, P. T. P., & Barrett, A. H. 1980, ApJ, 237, 38
Ho, P. T. P., & Townes, C. H. 1983, ARA&A, 21, 239

IRAS Point Source Catalog, Version 2. 1988, Joint *IRAS* Science Working Group (Washington, DC: GPO) (PSC)
Jennings, R. E., Cameron, D. H. M., Cudlip, W., & Hirst, C. J. 1987, MNRAS, 226, 461
Jones, B. F., & Herbig, G. H. 1979, AJ, 84, 1872
Knee, L. B. G., Cameron, M., & Liseau, R. 1990, A&A, 231, 419
Ladd, E. F. 1991, Ph.D. thesis, Harvard Univ.
Ladd, E. F., Lada, E. A., & Myers, P. C. 1993, ApJ, 410, 168
Ladd, E. F., Myers, P. C., & Goodman, A. A. 1994, in preparation
Langer, W. D., Wilson, R. W., Goldsmith, P. F., & Beichman, C. A. 1989, ApJ, 337, 355
Levreault, R. M. 1985, ApJ, 330, 897
Loren, R. B. 1976, ApJ, 209, 466
Loren, R. B., Vanden Bout, P. A., & Davis, J. H. 1973, ApJ, 185, L67
Lynds, B. T. 1969, PASP, 81, 496
McCaughrean, M. J. 1989, BAAS, 21, 712
Menten, K. M., & Walmsley, C. M. 1985, A&A, 146, 369
Myers, P. C. 1991, in Fragmentation of Molecular Clouds and Star Formation, ed. E. Falgarone, F. Boulanger, & G. Duvert (Dordrecht: Kluwer), 221
Myers, P. C., Ladd, E. F., & Fuller, G. A. 1991, ApJ, 372, L95
Sargent, A. I. 1976, ApJ, 233, 163
Schwartz, P. R., Frerking, M., A., & Smith, H. A. 1985, ApJ, 295, 89
Schwartz, P. R., Waak, J. A., & Smith, H. A. 1983, ApJ, 267, L109
Stacy, J. G., Benson, P. J., Myers, P. C., & Goodman, A. A. 1988, in Interstellar Matter: Proc. 2d Haystack Obs. Meeting, ed. J. M. Moran & P. T. P. Ho (New York: Gordon & Breach), 179
Strom, S. E., Grasdalen, G. L., & Strom, K. M. 1974, ApJ, 191, 111
Strom, S. E., Strom, K. M., & Carrasco, L. 1974, PASP, 86, 798
Strom, S. E., Vrba, F. J., & Strom, K. M., 1976, AJ, 81, 314
Tafalla, M., Bachiller, R., Martin-Pintado, J., & Wright, M. C. H., 1993, ApJ, 415, L139
Ungerechts, H., & Thaddeus, P. 1986, ApJS, 63, 645
Ungerechts, H., Walmsley, C. M., & Winnewisser, G. 1982, A&A, 111, 339
Wiseman, J. J., & Adams, F. C. 1994, ApJ, in press
Wouterloot, J. G. A., Walmsley, C. M., & Henkel, C. 1988, A&A, 203, 367